The role of oxidation damage in fatigue crack initiation of an advanced Ni-based superalloy

Cruchley, Sam; Li, Hangyue; Evans, Hugh; Bowen, Paul; Child, Dan; Hardy, Mark

DOI:
10.1016/j.ijfatigue.2015.08.016

Document Version
Peer reviewed version

Citation for published version (Harvard):
Cruchley, S, Li, H, Evans, H, Bowen, P, Child, D & Hardy, M 2015, 'The role of oxidation damage in fatigue crack initiation of an advanced Ni-based superalloy', *International Journal of Fatigue*, vol. 81, pp. 265-274. https://doi.org/10.1016/j.ijfatigue.2015.08.016

The Role of Oxidation Damage in Fatigue Crack Initiation of an Advanced Ni-based Superalloy

S. Cruchley, H.Y. Li, H.E. Evans, P. Bowen, D.J. Child, M.C. Hardy

PII: S0142-1123(15)00268-6
DOI: http://dx.doi.org/10.1016/j.ijfatigue.2015.08.016
Reference: JIJF 3692

To appear in: *International Journal of Fatigue*

Received Date: 20 April 2015
Revised Date: 13 August 2015
Accepted Date: 19 August 2015

Please cite this article as: Cruchley, S., Li, H.Y., Evans, H.E., Bowen, P., Child, D.J., Hardy, M.C., The Role of Oxidation Damage in Fatigue Crack Initiation of an Advanced Ni-based Superalloy, *International Journal of Fatigue* (2015), doi: http://dx.doi.org/10.1016/j.ijfatigue.2015.08.016

The Role of Oxidation Damage in Fatigue Crack Initiation of an Advanced Ni-based Superalloy

S.Cruchley[1], H.Y. Li[1*], H.E. Evans[1], P. Bowen[1], D.J. Child[2] and M.C. Hardy[2]

[1]School of Metallurgy and Materials, University of Birmingham, Birmingham, B15 2TT, UK

[2]Rolls-Royce plc, Derby, DE24 8BJ, UK

*Corresponding author
Hangyue Li
h.y.li.1@bham.ac.uk

Abstract

The effects of prior oxidation on the room temperature fatigue life of coarse-grained Ni-based superalloy, RR1000, have been investigated. High cycle fatigue tests were conducted, on both machined and pre-oxidised testpieces, at room temperature at an R ratio of 0.1. The oxidation damage was produced by pre-exposures at 700^{o}C for either 100 or 2000 hours. Pre-oxidised testpieces tended to fail with shorter fatigue lives than those obtained from the as-machined testpieces although they were also observed to outperform the as-machined test pieces at peak stress levels around 900 MPa. The chromia scale and intergranular alumina intrusions formed during pre-oxidation are prone to crack under fatigue loading leading to early crack nucleation and an associated reduction in fatigue life. This has been confirmed to be the case both below and above a peak stress level of ~900 MPa. The better fatigue performance of the pre-oxidised specimens around this stress level is attributed to plastic yielding of the weaker γ' denuded zone, which effectively eases the stress concentration introduced by the cracking of the chromia scale and intergranular internal oxides. This γ' denuded zone is also a product of pre-oxidation and develops as a result of the selective oxidation of Al and Ti. Over a limited stress range, its presence confers a beneficial effect of oxidation on fatigue life.

Keywords: Oxidation, Fatigue crack initiation, High cycle fatigue, RR1000

1. Introduction

The role of environmental degradation in the mechanical performance of a component is important, particularly for aero-engine rotor discs which operate in high temperature oxidising environments under significant external loads. When these Ni-based alloys oxidise, a protective chromia external scale is formed along with the sub-surface formation of alumina both intergranularly and intragranularly [1]. Beyond these is a weaker region depleted in γ′ particles (nominally $Ni_3(Al,Ti)$) and grain boundary carbides (nominally $M_{23}C_6$). The formation of these sub-surface internal oxides is undesirable and may have a significant detrimental effect on the mechanical properties of the alloy [2, 3]. It has been postulated that the internal oxides that form at the grain boundaries have the potential to crack and introduce local stress concentrations which promote early initiation and therefore reduce component lives [2]. Oxides are inherently brittle materials with tensile failure strains of <1% and K_{1c} values for chromia and alumina in the range of 0.4-2.0 $MPa.m^{1/2}$ [4]. These are typically much lower than the underlying alloy, so it should be no surprise that it is possible for these oxides to fail under tensile loading.

Several studies on the Ni-based superalloys ME3, and Udimet 720 have found that prior oxidation reduces fatigue life and, in IN100, that the crack initiation life was similar to the number of cycles to cause the oxide to fracture [5-7]. The tests performed on ME3, have shown that prior high temperature exposure in an oxidising environment (>700°C) for prolonged periods of time (100-2020 hours) have a detrimental effect on the high temperature (704°C) notched fatigue life [5]. The thicker the external scale and the deeper the internal damage the more pronounced the reduction in life [5] which was thought to be due to the dissolution of $M_{23}C_6$ particles. Removal of the internally oxidised region did not lead to a complete recovery in high temperature fatigue life but the removal of the carbide dissolution zone did. Another study [7] using extensive prior exposures of ME3 (704°C for 439 hours) and Udimet 720 (650°C and 704°C for 100 or 1029 hours) found that the mean lives of pre-oxidised specimens had up to a 70% reduction in high temperature LCF life. A change of crack initiation was also seen from sub-surface (as-received) to surface (pre-oxidised). Performing the prior exposures in vacuum led to no reduction in fatigue life, illustrating that oxidation damage is driving the reduction in life [7].

The aim of the present work was to extend the previous research and examine the potential for intergranular internal oxides to act as preferential crack initiation sites and therefore affect the overall life of a component. This work concentrates on the fundamental understanding of the initiation between oxidation and fatigue. The use of pre-oxidised samples undergoing fatigue at room temperature was performed to isolate the effect of oxidation on the fatigue life. This allows the

exclusion of any high temperature processes by removing the influence of creep deformation or oxidation ahead of the crack tip that would affect the fatigue crack growth. Bend samples have been used to restrict fatigue failures to the top surface region where the oxide resides.

2. Experimental Method

2.1. Material

A third generation, powder processed, γ' precipitation strengthened Ni-based superalloy, RR1000, was used in this study. The chemical composition of the alloy is given in Table 1. The material had received a supersolvus solution heat treatment and subsequent ageing treatment which produced a coarse-grained microstructure (30-50 μm) and a bi-modal dispersion of γ' precipitates.

2.2. Preparation of fatigue testpieces and pre-oxidation

High cycle fatigue testing was performed at room temperature under four-point bend loading using a rectangular bar testpiece geometry (100 mm x 9 mm x 10 mm). Testing was performed on either as-machined or pre-oxidised testpieces. In the as-machined condition the corners were chamfered to remove the potential for corner crack initiation and the specimens were subsequently cleaned and degreased in ethanol ultrasonically for a period of 5 minutes before testing. The surfaces of the specimens were left as-machined with the low stress ground machine marks parallel to the direction of the applied stress. The surfaces of the specimens for pre-oxidation, however, were prepared by grinding and polishing to a R_a = 0.3 μm, with the edges and corners chamfered to the same surface finish to reduce stress concentrations. These were again cleaned and degreased ultrasonically in ethanol for a period of 5 minutes. An Elite Thermal Systems Ltd. box furnace was pre-heated to 700^{o}C into which samples were placed for pre-oxidation in laboratory air for time periods of either 100 or 2000 hours. Calibration was performed using an N-type thermocouple to ±5^{o}C. Upon placing the specimens in the furnace a temperature drop of ~50^{o}C was recorded but the target temperature was regained within 10 minutes. A pre-oxidised (2000 hours) specimen was used to check the effect of the aged microstructure on fatigue life. This was performed by removing all of the oxidation damage (external and internal) by grinding using 240 grit paper. Grinding marks were parallel to the direction of the applied stress.

2.3. High cycle fatigue (HCF) testing

Testing was performed at room temperature under a four-point bending configuration with a maximum applied stress of between 700 - 1000 MPa. An Amsler Vibrophore HCF machine with a load capacity of 20 kN was employed and a frequency of ~75 Hz was achieved on the current testpiece geometry. A span ratio of 20:60 mm and a R ratio of 0.1 were utilised throughout.

Testpieces that had not failed after $5x10^7$ cycles were deemed to be a runout and the specimen was removed from the test machine for further analysis.

2.4. Fractographic and metallographic analysis

The fracture surfaces of failed specimens were examined in a Phillips XL-30 scanning electron microscope (SEM) in order to understand the influence of pre-oxidation on the fatigue process. The top surface of the specimen, which was subjected to tensile stress during testing, was also examined for any cracking of the oxide scale. Care was taken in the preparation of metallographic sections due to the brittle nature of the oxides. Specimens were first mounted whole under vacuum in a low shrinkage, low viscosity epoxy resin. The region of highest stress was then cut out using a precision cutting machine at a low cutting speed (<0.05 mm/min) before being re-mounted under vacuum in the same epoxy resin. Note that the section plane was parallel to the longitudinal direction and perpendicular to the top surface which had been subjected to tensile stress. Samples were then polished to a final stage of 0.25 μm diamond solution or OP-S colloidal silica solution before being cleaned ultrasonically in ethanol and imaged using a Jeol 7000F field emission gun (FEG) SEM. Chemical etching was performed by swabbing the surface of the sample for 30 seconds using Kalling's reagent or through a 60 second immersion in a selective γ′ etchant (compositions in Table II).

2.5. Nano-indentation and Microhardness

Nano-indentation was performed on a cross-section of a specimen oxidised for 500 hours at 800°C, using a Micromaterials Ltd. Platform 3 NanoTest machine. The indentations were performed at 1 μm intervals in a diagonal pattern across the specimen, starting within the Ni-plate and progressing through the oxide into the bulk alloy. The indents were performed using a Berkovich indenter under a load controlled setting to a maximum load of 30 mN. A loading rate of 1 mNs^{-1} was used. Once the indenter reached the maximum load this was then held for a short period of time (~30 seconds) before being removed from the specimen, giving a load vs. displacement graph. The hardness of the material was then calculated from the tangent to the unloading curve.

Vickers microhardness testing was also performed on a cross-section of an as-machined specimen and an aged specimen (oxide removed), using a Struers Durascan 50 automated microhardness machine. It was performed using a 0.3 kg load, with an average value being taken from 12 indents.

3. Results and Discussion

3.1. Surface oxidation damage caused by pre-oxidation

Previous studies on the Ni-based superalloys Udimet 720, ME3 and RR1000 under cyclic fatigue or dwell fatigue conditions found no change in oxide composition compared with the unstressed condition but did record an enhancement of the oxidation damage [7, 8]. This illustrates that using pre-oxidation as a method of isolating the effect of environmental damage on fatigue performance is a reasonable approach. The typical oxide morphology of the pre-oxidised RR1000 is complex, as shown in the cross-sections in Figure 1. A more detailed description of the oxidation damage and confirmation of the composition are provided in previous studies on this alloy [1, 9, 10]. The oxide is composed of a continuous external layer of chromia and extensive sub-surface formation of alumina, which penetrates the substrate both intergranularly and intragranularly. The intergranular penetrations are deeper and often continuous whereas the intragranular penetrations consist of smaller isolated particles within the grains. A significant γ′ denuded zone encompasses and exists ahead of this internal oxide. Ahead of this zone is a region within which the Cr-Mo rich grain boundary phase has dissociated (Figure 1 (c)). This phase is often assumed to be $M_{23}C_6$ carbides but could possibly be sigma phase [11]. The depth of each type of oxidation damage is shown in Table III for each exposure time. The oxidation damage increases in thickness and depth with increasing time and temperature, the kinetics of which are described elsewhere [1, 10].

Nano-indentation was performed (with an applied load of 30 nN) in order to evaluate the variation of mechanical properties across the different zones affected by pre-oxidation. Figure 2 shows the results from a sample after oxidation at 800°C for 500 hours. The hardness value of the external oxide layer is 7.4 GPa but this gradually reduces through the zone of internal oxidation until a minimum is reached in the γ′ denuded zone before increasing again into the matrix. Clearly a softer layer is sandwiched between the outer oxide shell and the matrix. It is reasonable to suggest that the reduction in yield stress in the γ′ denuded zone is proportional to the reduction in hardness values. The yield stress of the matrix is about 1010 MPa, hence the yield stress in the γ′ denuded zone can be estimated to be around 810 MPa (using the average hardness value in the γ′ denuded zone and in the matrix). The formation of this weaker region has been reported previously [5, 9, 10].

3.2. Comparison of fatigue lives

The results of room temperature high cycle fatigue (HCF) tests obtained using pre-oxidised and as-machined testpieces are compared in Figure 3. At a stress level of 700 MPa, all testpieces ran out at 5 x 10^7 cycles, indicating that this stress level is close to the fatigue endurance limit. The fatigue behaviour of the as-machined testpieces was broadly as expected but there was a typical level of

scatter in the results as can be appreciated from Figure 3. Some judgement is required in drawing a trend line but that shown in Figure 3, demonstrating a decrease in life with increasing stress above the fatigue endurance limit, seems reasonable. It is understood that the majority of total fatigue life of the as-received testpieces is spent on initiating fatigue cracks and early propagation near threshold, for such smooth and small laboratory testpieces [13]. This argument is supported by a simple estimation of propagation life from a natural defect size of 100 μm (measured ALA grain size) to catastrophic failure using a Paris law:

$$\frac{da}{dN} = C(\Delta K)^n \qquad (1)$$

where C = 1×10^{-10} and n = 3.81, with da/dN and ΔK in the units of mm/cycle and MPa√m. The numbers of cycles to failure at peak stress levels of 800, 900 and 1000 MPa were calculated to be 490000, 310000, and 210000 respectively (shown by a dashed line in Figure 3).

A sharp reduction in fatigue life of up to two orders of magnitude, compared with those of the as-machined testpieces, was observed in the pre-oxidised testpieces at a stress of 800 MPa. A larger reduction in life was seen with the longer pre-exposure, i.e. presumably with the associated increased depth of oxidation damage. With further increase in applied stress, the fatigue life of pre-oxidised testpieces *increased* instead of decreasing, as would have been expected from the behaviour found for the as-machined specimens. Such a trend continued up to an applied stress of 900 MPa where all the pre-oxidised testpieces ran out at $5\text{x}10^7$ cycles. At the highest stress level investigated here, 1000 MPa, a significant deficit in the fatigue life of the pre-oxidised testpieces was again evident. Comparing to the estimated proportional crack propagation life, it is clear that such a deficit comes from the small number of cycles required to initiate fatigue cracks for the pre-oxidised testpieces tested at 800 MPa and 1000 MPa.

In order to clarify whether ageing during the oxidation exposure has played any role in the fatigue behaviour of the pre-oxidised testpieces, a single test was undertaken using a pre-oxidised specimen (700°C for 2000 hours) with the top oxide scale and oxidation affected zone removed. The result is shown as the star symbol in Figure 3. The specimen failed at ~$1.3\text{x}10^7$ cycles, under a maximum stress of 900 MPa, which is consistent with the results observed for the as-machined testpieces. This is substantially less than the corresponding pre-oxidised samples which remained un-failed at $5\text{x }10^7$ cycles (Figure 3). This result, although limited, indicates that it is the oxidation process not microstructural ageing caused by prolonged exposure at 700°C that causes the increase in room temperature fatigue life at this relatively high stress level (900 MPa). In fact, significant microstructural changes may not have occurred during the pre-oxidation period since the

microhardness of both as-machined and the aged specimen were identical at 459 Hv (± 1 standard deviation of 6.1 for the aged material and 7.6 for the as-machined).

3.3. Fractography

The crack-initiation location in the as-machined specimen and pre-oxidised specimens are compared in Figure 4. At room temperature and in the high cycle fatigue regime, it is generally observed that slip bands tend to form in the larger grains and lead to the initiation of fatigue cracks although the contribution of neighbouring grains, by having nearly-similar Schmid factors, cannot be disregarded [12]. The crack initiation site observed in the current study for the as-machined specimens at 800 MPa was beneath the surface and associated with a relatively large grain facet (~60 μm) (Figure 4 (d)). Such large grains do not necessarily occur within the shallow high-stress layer at the top surface of the specimen and this variability is a possible reason for the large discrepancy in life at a maximum applied stress of 800 MPa in the as-machined condition. In all cases around the initiation site, fatigue crack growth demonstrated a faceted manner, which dictates the characteristics of the near threshold crack growth at room temperature. With further crack extension, the faceted crystallographic appearance is replaced with flat transgranular growth, which is typical of crack growth at higher stress intensity factor ranges, within the Paris regime. At high stresses, 900 MPa and 1000 MPa, the initiation site in the as-machined specimens shifted from sub-surface to the surface and only a single initiation site was recorded on the fracture surface. However, several surface-breaking cracks within the inner span region (confirmed on the cross-section analysis) illustrate the potential that more initiation sites were present but with only one dominating the fatigue life. Similarly, the aged specimen showed a similar surface initiation at a maximum applied load of 900 MPa.

The fatigue crack initiation sites of the pre-oxidised specimens occurred at the surface in all cases (Figure 4). Multiple surface initiation sites occurred on the fracture plane at a maximum applied stress of 1000 MPa (Figure 4(b&c)) but a single initiation was present at all other stresses. Apart from the location and distribution of these sites, the fracture surface morphology was very similar. This indicates that the oxides were the source of crack initiation whilst having little effect on room temperature fatigue crack *growth*. This is expected because the current investigation was deliberately carried out at room temperature to avoid potential interactions between the environment and crack growth behaviour. It is known, for example, that the crack propagation rate is increased and the crack path changes from transgranular to intergranular when high-temperature fatigue tests are conducted in air rather than vacuum [14-16].

In previous work using cylindrical specimens [7], a clear shift was found between sub-surface crack initiation without oxidation to surface initiation in the presence of oxides. This dramatic change was not generally found in the present bend tests because the highest in-plane stress was located at the

specimen surface. Nevertheless, near-surface crack initiation did occur in the unoxidised as-machined specimen at a stress of 800 MPa. In this case, the initiation site was associated with a large grain (Figure 4(d)).

3.4. Analysis of Metallographic Sections

Before preparing metallographic sections, the top surfaces of the tested specimens were examined under the SEM, to check whether there were any surface cracks present within the gauge section. Numerous cracks were found on all pre-oxidised specimens except those tested at 700 and 900 MPa. Surface-breaking cracks could also be observed near the fracture surface on the area of maximum tensile stress. These have been reported previously [20] for pre-oxidised specimens tested at 800 MPa but were found here at stresses of 900 and 1000 MPa in both pre-oxidised and as-machined testpieces (Figure 5). Note that the cracking of the external oxide scale was always perpendicular to the stressing direction, whereas it was around 45^{o} to the stressing direction in the as-machined testpieces. This indicates a different mode of failure, with crystallographic slip dominating in the as-machined testpieces and oxide cracking dominating in the pre-oxidised testpieces. No cracking of the external oxide was seen in the runout pre-oxidised samples tested at 700 MPa and 900 MPa.

Metallographic sections were prepared to provide insight into the crack initiation process in pre-oxidised testpieces and to identify the initiation sites. Figure 6(a) clearly shows a surface-breaking crack cutting through the external chromia scale, penetrating down an intergranular internal oxide and proceeding into the alloy in a pre-oxidised specimen (2000 hours) at a maximum applied stress of 800 MPa. A large number of similar cracks at 30-50 μm intervals occurred within the area of maximum stress, with each one being associated with an intergranular internal oxide. In all cases, these cut through the external chromia scale, penetrated down an intergranular internal oxide and proceeded into the alloy (Figure 6). Electron channelling contrast imaging and chemical etching were used to reveal the microstructure around these cracks. It was found that the cracks penetrated through the base alloy either by following a crystallographic facet (Figure 6 (b)) or the grain boundary (Figure 7) in the vicinity of the surface.

A large single crack was found in the shorter pre-oxidised condition (100 hours at 700^{o}C) at a maximum applied stress of 800 MPa (Figure 6 (c)). This crack seems to have originated in a similar manner as those in the longer pre-oxidation specimens, in that it cut through the external and intergranular internal oxide before progressing into the alloy by following crystallographic facets. This is not unexpected since the surface region is the area of highest tensile stress and these intergranular internal oxides are inherently sharp brittle features with low fracture toughness. The tensile failure strains (<1%) and fracture toughness of both chromia (K_{1c} ~ 2.0 MPa.m$^{1/2}$)[4] and

alumina (K_{1c} ~ 0.4-1.0 MPa.$m^{1/2}$) [4] are significantly lower than for the bulk alloy. It is then feasible that these oxides crack preferentially leading to early fatigue crack initiation at a maximum applied stress of 800 MPa and result in a deficit in total fatigue life.

This mechanism is supported by a previous study which found that surface oxide cracking and crack initiation are closely correlated [6] although it is currently unclear whether the surface or sub-surface oxide cracks first. No cracking of the external oxide occurred above an intragranular internal oxide at the stress of 800 MPa nor was any cracking of the intragranular oxides recorded at any stress. One reason that only the internal intergranular oxides crack is that these oxide intrusions are longer than the intragranular oxide particles. The anisotropic nature of deformation between neighbouring grains could also impose strain concentrations on the intergranular oxide intrusion. It is also now thought that such intrusions will develop stress fields during their formation because of the associated volume expansion on oxide formation and that enhanced tensile stresses will exist over part of the intrusion length [17, 18].

Above 800 MPa, an increase in fatigue life is found in the pre-oxidised specimens, with specimens at 825 and 850 MPa exhibiting longer lives and specimens at 900 MPa running out. This occurred in both of the pre-oxidised conditions (100 and 2000 hours at 700^{o}C). No cracks were visible in the sectioned 900 MPa specimen but cracks were seen in the external oxide scale in both the 825 and 850 MPa specimens. No cracks were observed beneath the external scale in the intragranular or intergranular internal oxides at maximum applied stresses between 825-900 MPa. Above this stress range, at a maximum outer fibre stress of 1000 MPa, failure occurred quickly (2-4x10^5 cycles) and numerous cracks were found in the area of maximum stress in both the external oxide scale and the intergranular alumina intrusions, often then penetrating further into the alloy (Figure 8). This behaviour indicates the stress, $\sigma_{f,}$ at and above which extensive failure of the oxide phases and within the particle-denuded zones lead to a catastrophic reduction in fatigue life.

Sudbrack et al. [5] suggested that failure within the carbide dissolution zone (e.g. Figure 7) was the main cause of the high temperature notched fatigue life deficit in the Ni-based superalloy ME3, where weakened grain boundaries were thought to be the sites of initiation at high temperature [5]. In the present case, the Cr-Mo rich grain boundary phase dissolution zone is present appreciably beyond the crack and internal oxides (Figure 7 and Table III) with the crack penetrating into this zone. It is thought that these Cr-Mo rich grain boundary phases are $M_{23}C_6$. It seems that these carbide-free grain boundaries could provide a weak path for the crack to propagate once it has initiated although they could also inhibit crack growth, at lower stresses, as a result of localised stress relaxation within the weaker grain boundary region.

3.5. Mechanisms

The level of stress within the chromia surface layer after pre-oxidation and prior to fatigue testing is not well established although it is expected to have a large in-plane compression component but further discussion is given later. One objective of the present work was to establish experimentally the room temperature applied tensile stress at which oxide cracking would be observed and, clearly, at 800 MPa (Figure 6) cracking of the oxide has occurred. At this stress level, the reduction in fatigue lifetimes resulting from pre-oxidation is also substantial (1-2 orders of magnitude) as can be seen in Figure 3. From the hardness measurements and estimated yield stress of this zone, as discussed earlier, it is expected that negligible yield will have occurred at this (and lower) stress levels and that cracks nucleated within the oxide will propagate readily across this zone and into the bulk alloy (Figures 6(c) and 7, for example). A deleterious effect of oxidation due to early crack nucleation results.

Within the higher stress range (σ_{max}, R=0.1) of 825-900 MPa, an increase in fatigue life for the pre-oxidised samples over those observed at 800 MPa was found. At the highest stress in this range (900 MPa) the fatigue life of the pre-oxidised samples is even longer than those of the as-received samples. This beneficial effect of pre-oxidation is considered to be related to yielding of the γ' denuded zone, for which a yield stress of about 810 MPa was estimated earlier based on hardness measurements. The associated plastic relaxation within this zone would inhibit cracking of the external oxide scale and/or crack propagation from the oxide to the bulk alloy (Figures 6(d) and (e) and lead to an improvement in fatigue endurance. Apparently such an effect will have its limit, however, and there certainly is a loss of the benefit of oxidation between 900 and 1000 MPa. At 1000 MPa, extensive cracking of the oxide scale occurs and a significant reduction in total fatigue life results; this damaging effect of oxidation is similar to that found at a stress level of 800 MPa. The mechanisms described above are captured in a schematic diagram in Figure 9.

Another schematic diagram comparing the fatigue lives of as-machined and pre-oxidised specimens is shown in Figure 10 in order to aid this present discussion. The shaded area in this diagram shows that the improvement in fatigue lives resulting from pre-oxidation exists only over a range of intermediate stresses. The lower stress, σ_y, is taken to be just above the yield stress of the γ' denuded zone and is between 800 and 825 MPa and it is only at and above this stress that relaxation processes within this zone can confer improvements in fatigue life. At and above the upper limit, σ_f, (between 900 and 1000 MPa), failure occurs rapidly in the pre-oxidised samples and short lifetimes arise. This stress may correspond to the UTS of the precipitate denuded regions so that, at higher levels of stress, the load-bearing capacity of the denuded zones is exceeded and early failure can be expected. It should be noted that these precipitate-free zones exist not only beneath the surface oxide but also along alloy

grain boundaries (Figure 7) where fast crack propagation might be expected at high stresses [5]. A schematic diagram for the mechanism of fatigue crack initiation in pre-oxidised specimens is shown in Figure 9. This illustrates that at an applied stress of 800 MPa and 1000 MPa cracking of the external oxide scale and intergranular internal oxides occurs, thus causing early crack initiation and a significant reduction in fatigue life over the as-machined condition.

One uncertainty in this discussion is the actual level of stress present in the outer region of the testpiece. A simple calculation based on the generation of differential thermal strains within a thin surface oxide layer having a planar interface with the alloy is given in the Appendix. This indicates that a large compressive stress of around 1.8 GPa would be expected to develop in-plane in the external scale upon cooling to room temperature after a pre-oxidation exposure at 700^{o}C. This seems unlikely, however, because there is clear evidence (e.g. Figure 6) that the chromia layer cracks in a tensile manner on the application of a stress of only 800 MPa. The corresponding in-plane tensile strain is ~0.3% (calculated using a Young's modulus for chromia of 270 GPa) and this falls within the range of values (0.002-0.95%) of the tensile fracture strain of chromia variously reported in the literature [19]. This wide range probably reflects a range in the length of crack-like defects within the oxide. This agreement suggests that the actual strain at room temperature in the oxide layer of the pre-oxidised specimens is essentially zero and that the imposed values of stress during fatigue testing and used in this discussion are realistic. The discrepancy with the simple calculation undertaken in the Appendix may be associated with a number of factors such as the non-planarity of the oxide/metal interface, the ability of the underlying γ' denuded zone to relax stresses both at temperature and during cooling, and the development of compressive in-plane stresses sub-surface during the formation of alumina intrusions. Clearly, further work will be needed to clarify the actual processes involved.

4. Concluding Summary

The effects of prior oxidation on the fatigue performance of a coarse-grained RR1000 have been studied at room temperature using four-point bend rectangular testpieces. The following conclusions can be drawn.

- Pre-oxidation at 700^{o}C in air for either 100 or 2000 hours produced a continuous surface oxide scale mainly composed of a protective chromia layer, approximately 1.5 μm thick, after the longer exposure period. Sub-surface, both intergranular and intragranular intrusions of alumina were also present with the former extending to ~3 μm beneath the surface oxide layer at the longer exposure time. Ahead of the zone of internal oxidation was a region depleted in γ' precipitates and this region was notably softer in microhardness than the bulk alloy.

- At applied surface stresses less than ≤ 800 MPa and at 1000 MPa, pre-oxidation appreciably reduced fatigue lives compared with as-machined specimens. Unexpectedly, at stresses intermediate between these values, pre-oxidation resulted in an enhancement of fatigue lives. This benefit of pre-oxidation is attributed to plastic yielding of the weaker γ′ denuded zone which either effectively relaxes the stress concentration introduced by the cracking of the chromia scale and intergranular internal oxides or prevents cracking of the external oxide/intergranular internal oxides.

- The fatigue-life deficit in the pre-oxidised specimens at the lower applied stresses (≤ 800 MPa) was associated with a change in crack initiation location from sub-surface (in as-machined specimens) to surface sites. This indicated that oxidation and not crystallographic facets was the cause of early crack nucleation in the pre-oxidised samples.

- At the higher applied stress (1000 MPa) the fatigue-life deficit was associated with rapid crack propagation through the γ′ depleted zone and along grain boundary paths depleted in $M_{23}C_6$ precipitates. It is likely that such large stresses exceed the UTS of the matrix alloy in the absence of particulate phases.

Acknowledgements

The authors acknowledge, with thanks, Prof. H. Dong for the provision of the nano-indentation equipment. The financial support provided by the Engineering and Physical Sciences Research Council (EPSRC) and Rolls-Royce plc. are also gratefully acknowledged.

References

[1] M.P. Taylor, H.E. Evans, S. Stekovic, M.C. Hardy, The oxidation characteristics of the Ni-base superalloy, RR1000, at temperatures 700-900°C, Materials at High Temperatures, 29 (2012) 145-150.

[2] F.H. Stott, G.C. Wood, Internal oxidation, Materials Science and Technology, 4 (1988) 1072-1078.

[3] R.A. Rapp, Kinetics, microstructures and mechanism of internal oxidation - its effect and prevention in high temperature alloy oxidation, Corrosion 21 (1965) 382-401.

[4] H.E. Evans, Stress effects in high temperature oxidation of metals, International Materials Reviews, 40 (1995) 1-40.

[5] C.K. Sudbrack, S.L. Draper, T.T. Gorman, J. Telesman, T.P. Gabb, D.R. Hull, Oxidation and the effects of high temperature exposures on notched fatigue life of an advanced powder metallurgy disk superalloy, in: E.S. Huron, R.C. Reed, M.C. Hardy, M.J. Mills, R.E. Montero, P.D. Portella, J. Telesman (Eds.) Superalloys 2012: 12th International Symposium on Superalloys, TMS, Seven Springs, PA, 2012, pp. 863-872.

[6] M. Reger, L. Remy, Fatigue oxidation interaction in IN-100 superalloy Metallurgical Transactions A - Physical Metallurgy and Materials Science, 19 (1988) 2259-2268.

[7] T.P. Gabb, J. Telesman, P.T. Kantzos, J.W. Smith, P.F. Browning, Effects of high temperature exposures on fatigue life of disk superalloys, in: K.A. Green, T.M. Pollock, H. Harada, T.E. Howson, R.C. Reed, J.J. Schirra, S. Walston (Eds.) Superalloys 2004: 10th international symposium on superalloys, TMS, Seven Springs, PA, 2004, pp. 269-274.

[8] A. Karabela, L.G. Zhao, J. Tong, N.J. Simms, J.R. Nicholls, M.C. Hardy, Effects of cyclic stress and temperature on oxidation damage of a nickel-based superalloy, Materials Science and Engineering: A, 528 (2011).

[9] S. Cruchley, H.E. Evans, M.P. Taylor, M.C. Hardy, S. Stekovic, Chromia layer growth on a Ni-based superalloy: Sub-parabolic kinetics and the role of titanium, Corrosion Science, 75 (2013) 58-66.

[10] S. Cruchley, M.P. Taylor, H.E. Evans, M.C. Hardy, D.J. Child, Characterisation of subsurface oxidation damage in Ni based superalloy, RR1000, Materials Science and Technology, 30 (2014) 1884-1889.

[11] R.J. Mitchell, C.M. Rae, S. Tin, Grain boundary transformations during isothermal exposure of powder metallurgy nickel base superalloys for turbine disc applications, Materials Science and Technology, 21 (2005) 125-132.

[12] K. Kobayashi, K. Yamaguchi, M. Hayakawa, M. Kimura, High-temperature fatigue properties of austenitic superalloys 718, A286 and 304L, International Journal of Fatigue, 30 (2008) 1978-1984.

[13] S. Suresh, Fatigue of Materials, Cambridge University Press, 1998.

[14] H.S. Kitaguchi, H.Y. Li, H.E. Evans, R.G. Ding, I.P. Jones, G. Baxter, P. Bowen, Oxidation ahead of a crack tip in an advanced Ni-based superalloy, Acta Materialia, 61 (2013) 1968-1981.

[15] H.W. Liu, Y. Oshida, Grain boundary oxidation and fatigue crack growth at elevated temperatures, Theoretical and Applied Fracture Mechanics, 6 (1986) 85-94.

[16] E. Andrieu, R. Molins, H. Ghonem, A. Pineau, Intergranular crack tip oxidation mechanism in a nickel-based superalloy, Materials Science and Engineering: A, 154 (1992) 21-28.

[17] H.E. Evans, H.Y. Li, P. Bowen, A mechanism for stress-aided grain boundary oxidation ahead of cracks, Scripta Materialia, 69 (2013) 179-182.

[18] K. Chan, Time-Dependent Crack Growth Thresholds of Ni-Base Superalloys, Metall and Mat Trans A, 45 (2014) 3454-3466.

[19] M. Schutze, S. Ito, W. Przybilla, H. Echsler, C. Bruns, Test methods and data on the mechanical properties of protective oxide scales, Materials at High Temperatures, 18 (2001) 39-50.

[20] I. Saeki, T. Ohno, D. Seto, O. Sakai, Y. Sugiyama, T. Sato, A. Yamauchi, K. Kurokawa, M. Takeda, T. Onishi, Measurement of Young's modulus of oxides at high temperature related to the oxidation study, Materials at High Temperatures, 28 (2011) 264-268.

[21] J. Robertson, M.I. Manning, Limits to adherence of oxide scales, Materials Science and Technology, 6 (1990) 81-92.

[22] M. Schütze, Protective oxide scales and their breakdown, Wiley, 1997.

Appendix

Calculation of the thermal stress induced in the external chromia oxide scale upon cooling from 700°C.

The in-plane stress can be estimated for thin oxides on a thick substrate using the following equation [4]:

$$\sigma_{ox} = \frac{-E_{ox}\ \Delta T\ (\alpha_{met} - \alpha_{ox})}{1 - v_{ox}} \quad (1)$$

where, σ_{ox} is the in-plane stress in the oxide layer, E_{ox} is the Young's modulus of the oxide, α_{met} and α_{ox} are the thermal coefficient of expansion of the metal and oxide respectively, ΔT is the temperature change (initial temperature minus final temperature) and v_{ox} is the Poisson's ratio of the oxide. In the case here parameters for the thermal co-efficient of thermal expansion are shown in Table IV. Assuming a room temperature of 20°C (293 K) a temperature drop of 680 K would occur. The Young's modulus of chromia is 275 GPa [20] and has a Poisson's ratio of 0.29 [21]. The in-plane compressive stress developed during cooling would be 1.8 GPa.

Table captions:

Table I: Nominal composition of RR1000 in both atomic and weight %.

Table II: Composition of two chemical etchants.

Table III: Oxidation damage measurements, in microns, of both pre-oxidation conditions, 700°C for 100 and 2000 hours (±1 standard deviation).

Table IV: Coefficients of thermal expansion [21, 22].

Figure captions:

Figure 1: BSE image of the cross-section through the typical oxidation damage produced by high temperature exposures at 700°C for a) 100 hours and b) 2000 hours etched with a selective γ′ etchant (Table II). c) A secondary electron image of a cross-section through sample oxidised at 700°C for 2000 hours clearly showing the Cr-Mo rich grain boundaries phase dissolution, sample was etched using Kalling's reagent.

Figure 2: a) BSE images of three of the nano-indentations performed, one in the internal oxide and two in the γ′ denuded region. b) Hardness (GPa) for each nano-indentation, with the dotted line showing the average for that region and illustrating that the γ′ denuded region is softer than the base alloy and similar to pure Ni.

Figure 3: A graph depicting the four conditions (as-received, aged, 100h pre-oxidation and 2000h pre-oxidation) tested showing maximum applied stress against number of cycles to failure. An arrow underneath the symbol demonstrates a runout test at 5 x 10^7 cycles. The trend lines of total life and the estimated proportional propagation life, without the influence of pre-oxidation, are shown as dashed lines.

Figure 4: Secondary electron images of the fracture surfaces of a) a 2000 hour pre-oxidised specimen that failed after 6x10^5 cycles at 800 MPa, b) multiple initiation sites from a 2000 hour pre-oxidised specimen that failed after 2x10^5 cycles at 1000 MPa, c) fatigue crack morphology at one initiation site from a 2000 hour pre-oxidised specimen that failed after 2x10^5 cycles at 1000 MPa, d) as-machined specimen failed at 1.1x10^7 million cycles at 800 MPa showing a sub-surface initiation and e) a 2000 hour pre-oxidised specimen that failed at 2.9x10^7 million cycles at 850 MPa. An arrow on each image indicates the crack initiation point.

Figure 5: Secondary electron images of surface breaking cracks in a) A pre-oxidised (2000h at 700°C) that failed at $3.7x10^7$ cycles at a maximum applied stress of 850 MPa and b) an as-machined specimen that failed after $9.6x10^6$ cycles at 900 MPa. The direction of the applied stress is parallel to the machining marks and indicated.

Figure 6: Images (BSE unless stated otherwise) of cross-sections through the area of maximum tensile stress showing: a) a crack through an intergranular alumina penetration of a pre-oxidised specimen (2000 hours) that failed after $1.9x10^6$ cycles at 800 MPa, b) a crack through an intergranular alumina penetration of the same sample as a) taken using electron channelling contrast imaging (ECCI), c) a pre-oxidised specimen (100 hours) that failed after $3.9x10^6$ cycles at 800 MPa, d) a pre-oxidised specimen (2000 hours) that failed after $1.2x10^7$ cycles at 825 MPa showing cracks only in the external chromia oxide, e) a pre-oxidised specimen (2000 hours) that failed after $3.7x10^7$ cycles at 850 MPa again showing cracks only in the external chromia oxide and f) a pre-oxidised specimen (2000 hours) that did not fail at 900 MPa.

Figure 7: BSE image of an etched pre-oxidised (2000h) specimens that failed after $1.9x10^6$ cycles at a maximum applied stress of 800 MPa, showing cracking of the external and intergranular internal oxide along with the presence of both a γ' denuded zone and carbide dissolution zone.

Figure 8: BSE images of a cross-section through the area of maximum tensile stress of a pre-oxidised specimen (2000 hours) that failed after $2x10^5$ cycles at 1000 MPa, showing a) an overview of a small crack and a large crack both emanating from the surface and b) a higher magnification image of the highlighted region showing the crack progressing through internal alumina and into the alloy.

Figure 9: Schematic diagram of the mechanism of crack initiation in a pre-oxidised sample occurring a) above the predicted γ' denuded zone yield stress, with no crack initiation occurring just cracking of the external oxide scale and b) below the predicted γ' denuded zone yield stress where cracking of the external oxide scale, intergranular internal oxide and the alloy have occurred. Cross-section was etched with Kalling's reagent (Table II)

Figure 10: Schematic diagram of the room temperature high cycle fatigue performance of RR1000, in both the as-machined and pre-oxidised conditions. The highlighted grey area is where the pre-oxidised condition exhibits a larger life than the as-received. σ_y indicates the yield stress of the γ' denuded zone, σ_f indicates where above this catastrophic failure occurs and σ_l indicates the fatigue limit.

Table I

	Ni	Co	Cr	Mo	Ti	Al	Ta	Hf	Zr	C	B
Weight %	Bal	18.5	15.0	5.0	3.6	3.0	2.0	0.5	0.06	0.02	0.03
Atomic %	Bal	17.9	16.5	3.0	4.3	6.35	0.63	0.16	0.04	0.14	0.10

Table II

	Gamma Prime (γ′) Etch	Kallings Etch
Chemical composition	Part 1 – 150 ml H_2O, – 150 ml HCl – 2.5 g MoO_3 Part 2 – 15 ml HNO_3 – 25 ml H_2O – 30 ml Part 1.	– 100 ml ethanol 96% – 100 ml hydrochloric acid 32% – 5 g copper (II) chloride

Table III

Units in μm	**External oxide scale**	**Internal oxide**		**γ′ denuded zone**		**Carbide dissolution**
		Intragranular	**Intergranular**	**Intragranular**	**Intergranular**	
100 hours	0.84 (±0.21)	0.80 (±0.27)	1.55 (±0.26)	1.04 (±0.29)	2.52 (±0.56)	-
2000 hours	1.48 (±0.86)	2.06 (±0.46)	2.92 (±0.48)	2.11 (±0.32)	3.72 (±0.72)	14.50 (±1.81)

Table IV

Material	Coefficient of thermal expansion (10^6 K^{-1})	T (^{o}C)
Cr_2O_3	8.5	400-800
Al_2O_3	8.1	400-800
Nimonic 75	15.4	20-700
CMSX 6	15.8	-

Figure 1

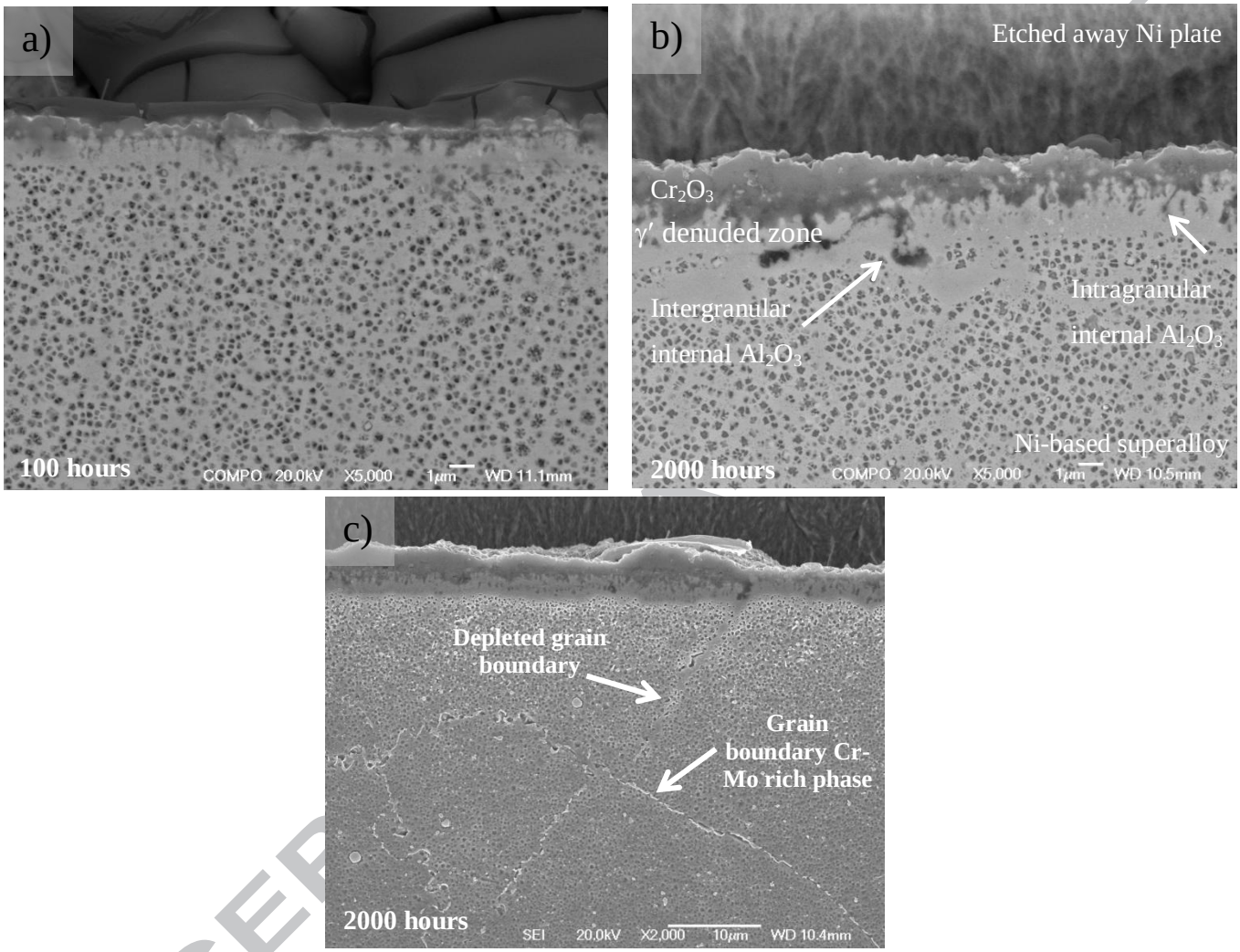

Figure 2

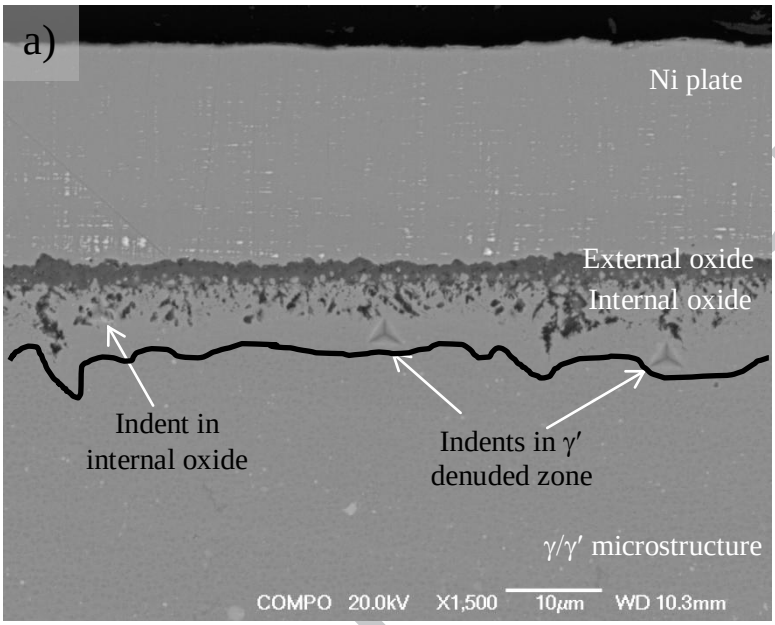

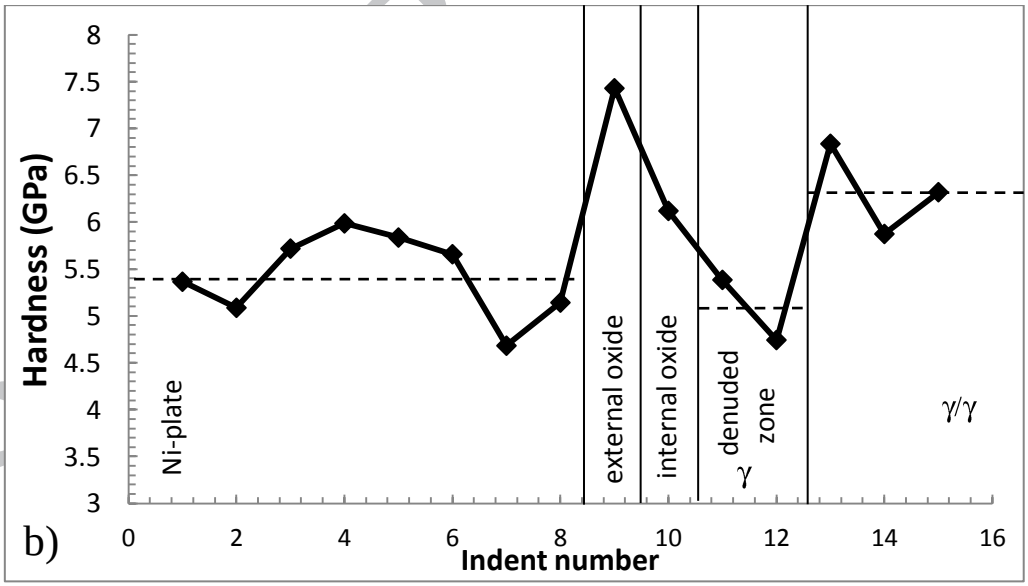

Figure 3

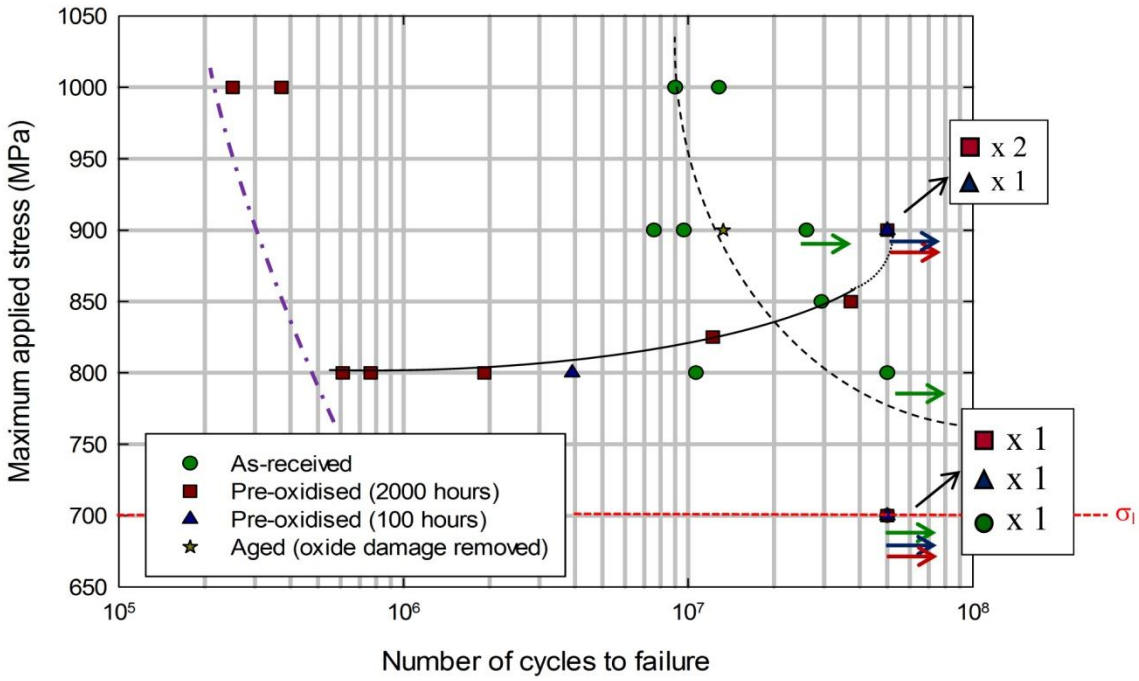

Figure 4

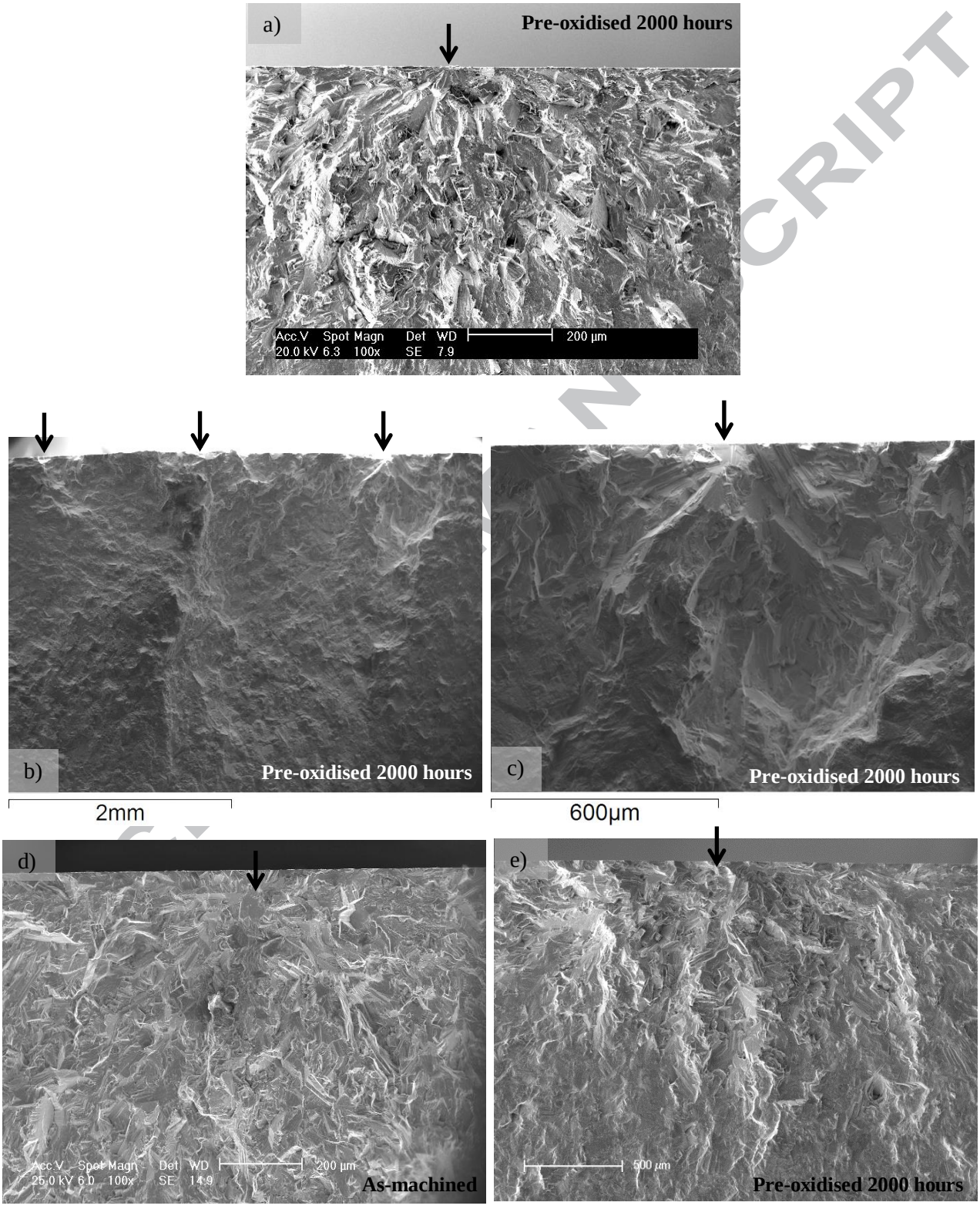

Figure 5

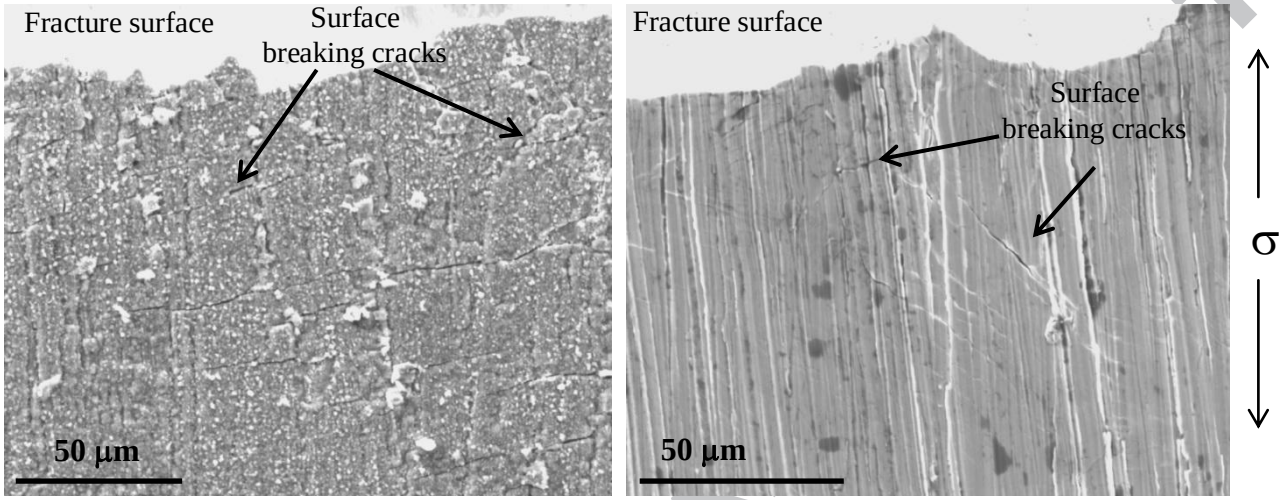

Figure 6

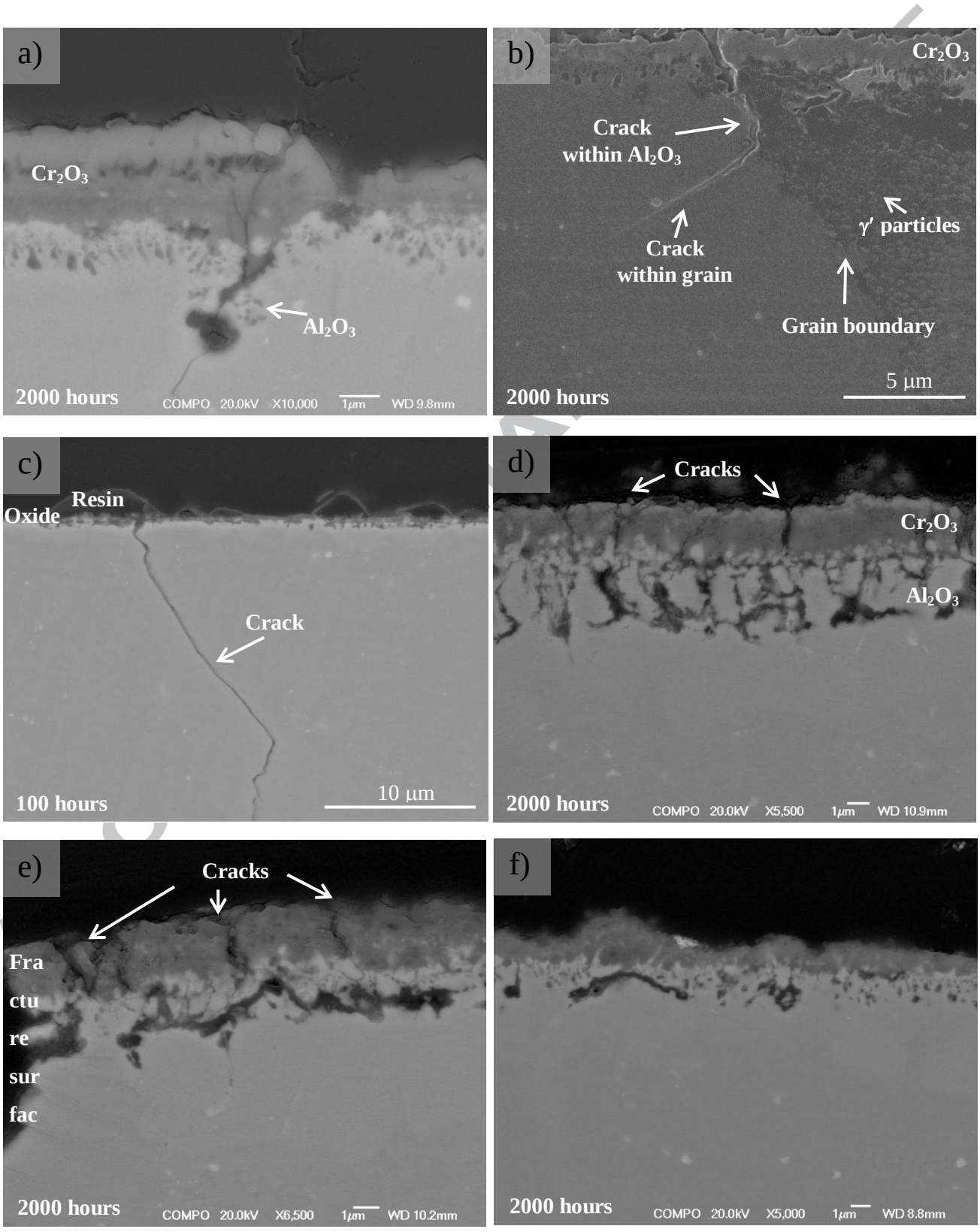

Figure 7

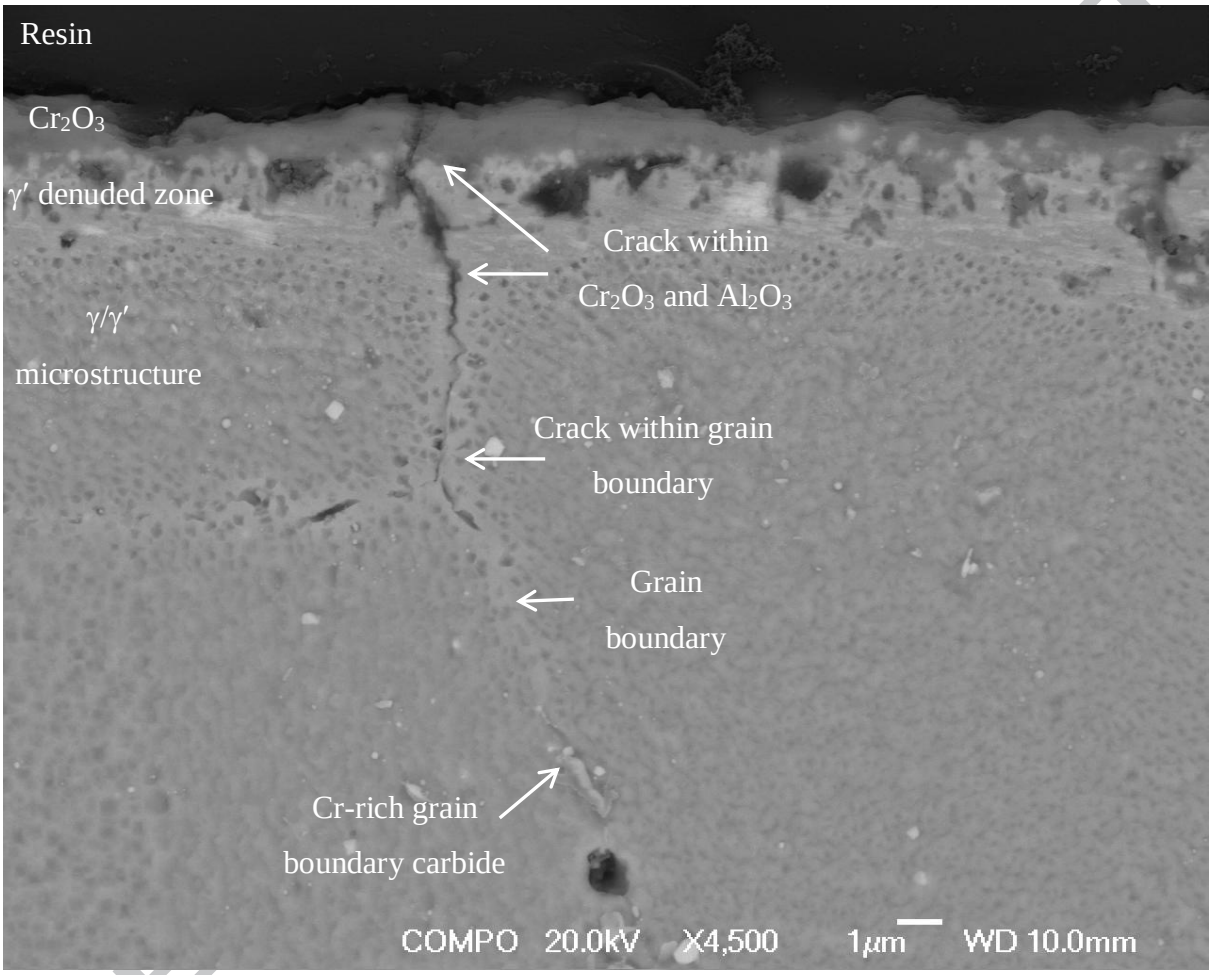

Figure 8

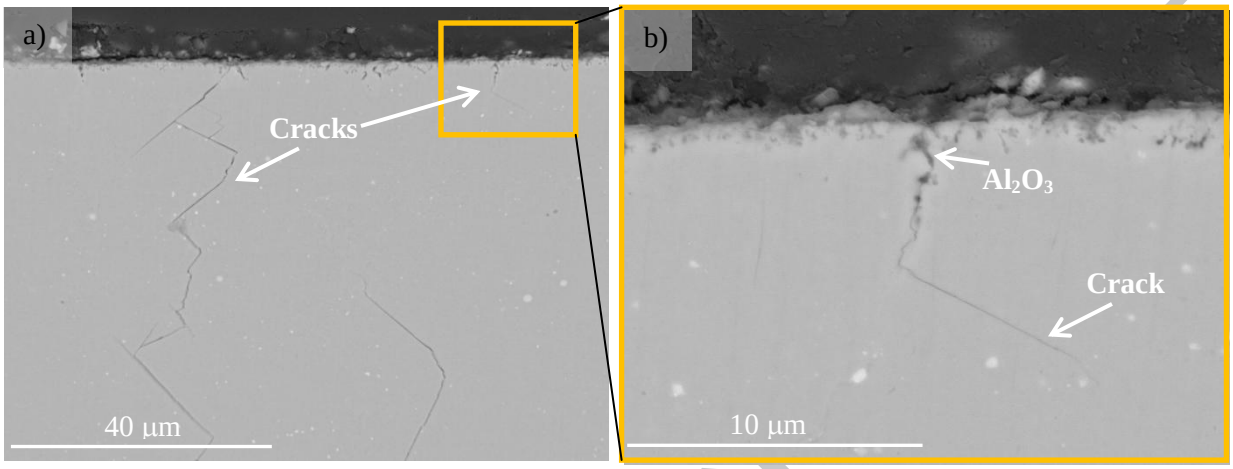

Figure 9

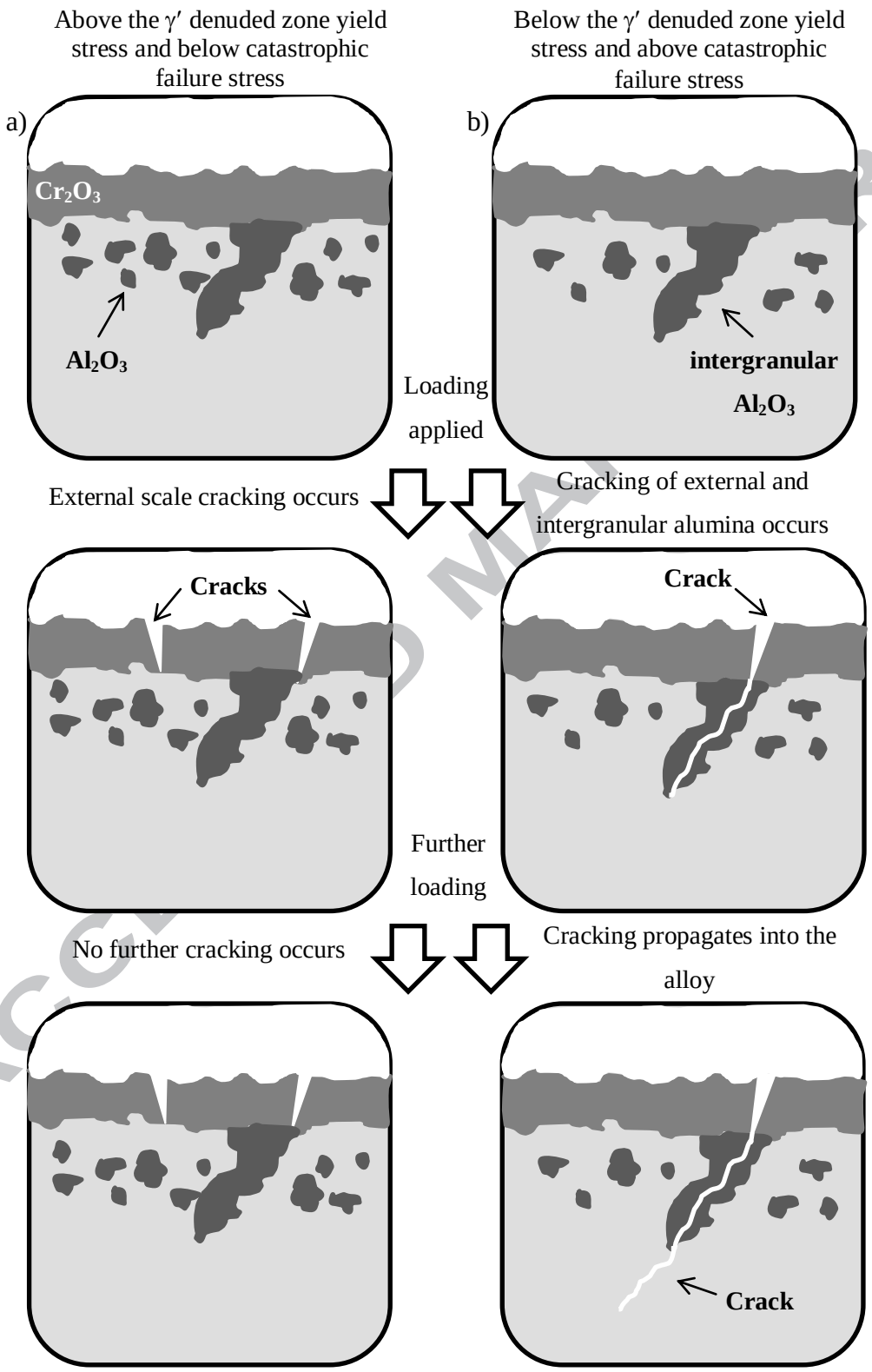

Figure 10

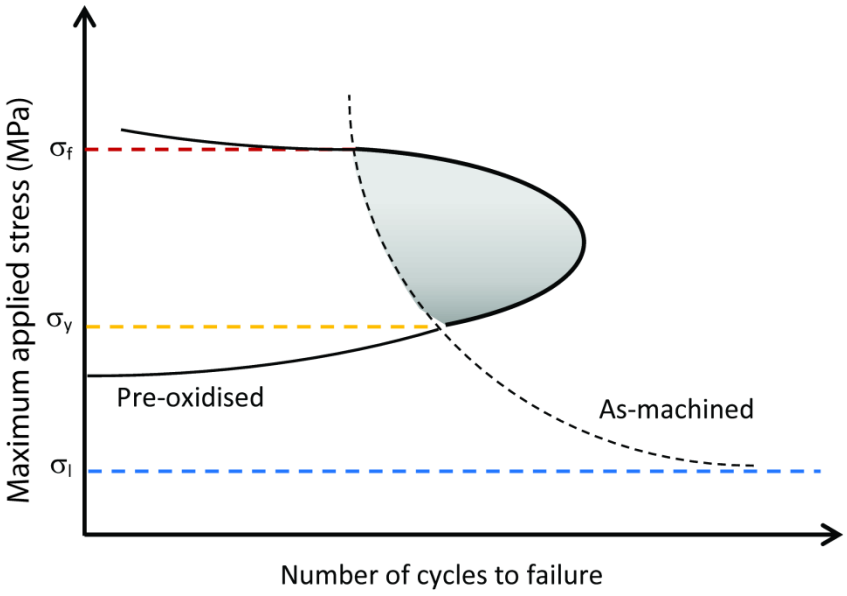

Highlights

Pre-oxidised Ni-based superalloy RR1000 was tested under high cycle fatigue at room temperature

Both negative and positive effects of pre-oxidation are observed

The critical stress of oxide cracking under fatigue (R=0.1) is between 700 and 800 MPa

Improved fatigue strength is also observed above this critical stress and is optimised at 900 MPa

Mechanisms for contrasting effects are proposed